GEOPHYSICS, VOL. 75, NO. 3 (MAY-JUNE 2010); P. F63–F70, 7 FIGS., 3 TABLES.
10.1190/1.3378765

Determining the orientation of marine CSEM receivers using orthogonal Procrustes rotation analysis

Kerry Key[1] and Andrew Lockwood[2]

ABSTRACT

Electromagnetic receivers deployed to the seafloor for CSEM surveys can have unknown orientations because of the unavailability of compass and tilt recordings. In such situations, only the orientation-independent parameters derived from the measured CSEM field vector can be interpreted, and this may result in less structural resolution than possible when the sensor orientations are known. An orthogonal Procrustes rotation analysis (OPRA) technique can be used to estimate the full 3D receiver orientation for inline and off-line CSEM receivers. The generality of this method allows it to be easily embedded into nonlinear CSEM inversion routines so that they iteratively search for both the receiver orientation and a seafloor electrical-conductivity model compatible with the data. Synthetic tests using the OPRA method jointly with a 1D inversion demonstrate that it can recover the rotation and tilt angles to about one degree accuracy for 1D data and to within a few degrees for 2D data. Application of this method to real survey data shows good agreement with a previous orientation method that is suitable only for determining the horizontal rotation of inline receivers. CSEM data collected over the Pluto gas field offshore the northwest coast of Australia were used to demonstrate how the OPRA method can be used to orient CSEM receivers prior to inversion of only the inline electric- and crossline magnetic-field components.

INTRODUCTION

The marine controlled-source electromagnetic (CSEM) method is a tool for remotely mapping the seafloor electrical-conductivity structure. Academics invented the method nearly three decades ago to study the oceanic lithosphere. More recently, CSEM has been heavily applied for hydrocarbon exploration on the continental shelves (e.g., Ellingsrud et al., 2002; Edwards, 2005; Constable and Srnka, 2007). CSEM survey data are commonly recorded by seafloor receivers outfitted with horizontal electric- and magnetic-field sensors (e.g., Constable et al., 1998), whereas more recent instrumentation also uses vertical electric- and magnetic-field sensors. Typically, the receivers are deployed from a survey vessel and then free-fall to the seafloor. On arrival at the seabed, the electric and magnetic sensor axes will be rotated to some arbitrary horizontal orientation and may also be tilted vertically due to regional seafloor topography or local rugosity.

Although in principle the sensor orientations can be recorded by electronic compasses and tiltmeters, these data are not always available. Furthermore, compass data are sometimes unreliable because of distortions from nearby magnetized receiver components such as the magnetic cores used in magnetometers or the inadvertent magnetization of the battery packs used to power the compass and data logger. Thus it is common to encounter CSEM survey data where at least some of the receiver orientations are either unknown or unreliable.

When the receiver orientation is unknown, one way to proceed is to decompose the data into its polarization-ellipse parameters (e.g., Smith and Ward, 1974). The maximum and minimum components of the polarization ellipse can be estimated independently of the ellipse orientation angle and have been used as robust interpretational quantities for many past CSEM surveys (e.g., MacGregor et al., 2001; Weitemeyer et al., 2006). However, the polarization-ellipse orientation can be indicative of seafloor conductivity variations, particularly for 2D and 3D structures that modify current flow from a basic dipole geometry. Therefore, some interpretational information is lost by ignoring this parameter, which is equivalent to ignoring the absolute orientation of the sensor axes.

Mittet et al. (2007) present a technique that determines the horizontal receiver orientation by rotating the electric-field vector until the crossline component is minimized. Although this method has often been effective for the standard inline acquisition geometry, it is not suitable for off-line receivers and can fail when the transmitter dipole does not point along the towpath (e.g., when lateral sea currents push the head or tail of the antenna off-line). In addition, this

Manuscript received by the Editor 7 July 2009; revised manuscript received 17 October 2009; published online 21 April 2010.
[1]University of California San Diego, Scripps Institution of Oceanography, La Jolla, California, U.S.A. E-mail: kkey@ucsd.edu.
[2]Woodside Energy Limited, Perth, Australia. E-mail: Andrew.Lockwood@woodside.com.au.
© 2010 Society of Exploration Geophysicists. All rights reserved.

method is not suitable for determining the receiver tilt angles.

Another technique for determining the receiver orientation is to perform polarization-ellipse matching, in which the data polarization ellipses are rotated until they match the polarization ellipses predicted by a forward model, thereby yielding an estimate of the receiver orientation. However, the ellipse orientation can be strongly dependent on seafloor conductivity. For example, Figure 1a shows the difference in polarization angles computed for 1- and 2-ohm-m half-spaces. For off-line receivers, the polarization angles exhibit as much as a 20° difference. Thus, one would need a priori knowledge of the seafloor conductivity to obtain reliable orientation estimates.

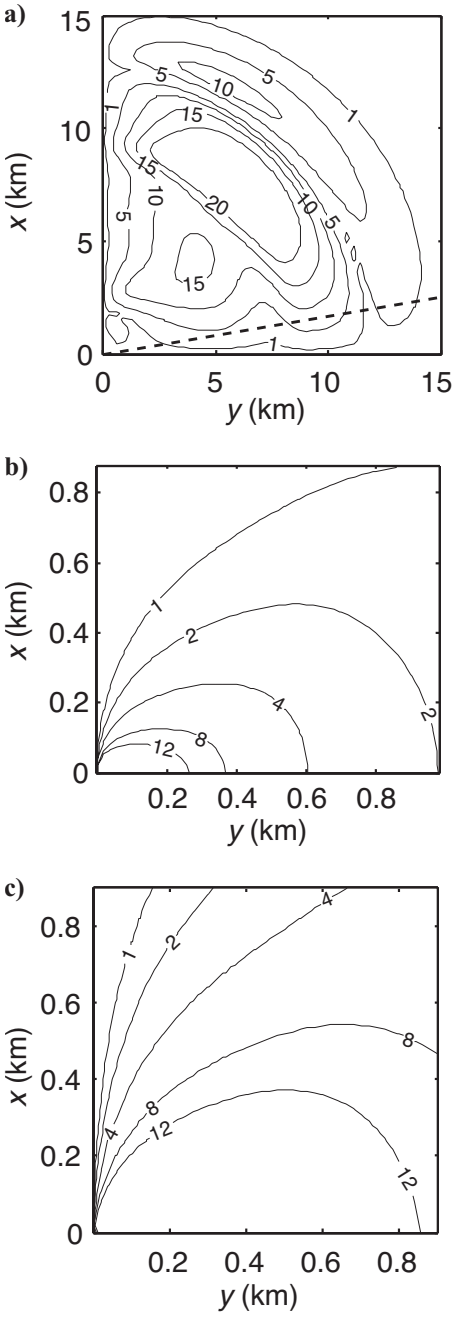

Figure 1. (a) Absolute difference in the orientation angle of the polarization-ellipse maximum for 1- and 2-ohm-m half-space models with a 0.25-Hz dipole antenna centered at (0,0) and pointing along y. Dashed line shows a receiver profile corresponding to a 10° antenna feather angle. (b) Difference in the polarization angle for a 20-m perturbation of the transmitter location along x. Only short offsets are shown. (c) Difference in the polarization angle for a 100-m perturbation of the transmitter location along x. Contour units are degrees.

For inline receivers, the 1D polarization-ellipse orientation in the horizontal plane is independent of seafloor conductivity, and thus polarization-ellipse matching has been commonly employed for determining the horizontal rotation of inline receivers. However, for transmitters with nonzero feather angles, inline receivers effectively become off-line receivers. The dashed line in Figure 1a shows an example in which a 10° transmitter feather angle could lead to several degrees of difference in polarization angle for 1- and 2-ohm-m half-spaces.

At short offsets (<1 km), the polarization angles are largely independent of seafloor conductivity, making short-offset data enticing for polarization-ellipse matching. However, the polarization angles at these ranges are very sensitive to uncertainties in the navigated transmitter position. Figure 1b and c shows examples in which the ellipse orientations change by as much as several degrees for 20- and 100-m off-line perturbations in transmitter position. Unless the transmitter position is known to within a few meters, short-offset data are unlikely to provide reliable orientation estimates.

Because polarization angles at longer offsets are dependent on seafloor conductivity, a logical solution is to pursue methods that couple the receiver orientation estimation with the data inversion for seafloor conductivity. Here we propose such a technique and demonstrate that it can provide reliable estimation of the receiver's horizontal rotation and tilt angles for inline and off-line receivers. Our technique is based on the orthogonal Procrustes rotation method that is commonly used for data-alignment problems in statistics, rigid-body rotations, and image analysis (e.g., Gower, 1975; Goodall, 1991; Challis, 1995). The Procrustes method is quite simple (e.g., Golub and Van Loan, 1996) and can easily be embedded into many commonly used inversion methods. Here we show its effectiveness when used with the Occam1DCSEM inversion (Key, 2009), but ultimately, we expect the best performance to be obtained when this method is implemented with 2D and 3D CSEM inversions.

METHODOLOGY

Orthogonal Procrustes rotation analysis

Consider the orientation of a marine CSEM receiver on the seafloor. The horizontal sensor axes (x',y') will be rotated by an unknown angle θ with respect to the survey reference coordinate system (x,y), as shown in Figure 2. Similarly, the receiver may be located on sloping topography or locally rugose seafloor, and the sensors might be tilted into the axes (x'',y'',z'') by angles α and β. The vector electric- and magnetic-field data $(\mathbf{F}'')$ recorded in the receiver's rotated coordinate system are related to the noise-free fields $(\mathbf{F})$ in the survey coordinate system by a 3×3 orthogonal rotation matrix $\mathbf{R}$ as

$$\mathbf{F}'' = \mathbf{F}\mathbf{R} + \mathbf{N}, \tag{1}$$

where $\mathbf{N}$ is an array representing noise in the field data. For n discrete source-receiver offsets, $\mathbf{F}$ and $\mathbf{F}''$ can be written as $2n\times3$ real valued matrices:

$$\mathbf{F} = \begin{bmatrix} \mathrm{Re}(F_{x,1}) & \mathrm{Re}(F_{y,1}) & \mathrm{Re}(F_{z,1}) \\ \mathrm{Im}(F_{x,1}) & \mathrm{Im}(F_{y,1}) & \mathrm{Im}(F_{z,1}) \\ \vdots & \vdots & \vdots \\ \mathrm{Re}(F_{x,n}) & \mathrm{Re}(F_{y,n}) & \mathrm{Re}(F_{z,n}) \\ \mathrm{Im}(F_{x,n}) & \mathrm{Im}(F_{y,n}) & \mathrm{Im}(F_{z,n}) \end{bmatrix}, \quad (2)$$

where $F_{x,i}$ specifies the x component of the ith datum, and the real and imaginary parts of the complex data have been separated into alternating rows. The rotation matrix $\mathbf{R}$ can be written as a product of rotations about individual axes:

$$\mathbf{R} = \mathbf{R}_z \mathbf{R}_{y'} \mathbf{R}_{x''}, \quad (3)$$

where

$$\mathbf{R}_z = \begin{bmatrix} \cos(\theta) & -\sin(\theta) & 0 \\ \sin(\theta) & \cos(\theta) & 0 \\ 0 & 0 & 1 \end{bmatrix}, \quad (4)$$

$$\mathbf{R}_{y'} = \begin{bmatrix} \cos(\alpha) & 0 & -\sin(\alpha) \\ 0 & 1 & 0 \\ \sin(\alpha) & 0 & \cos(\alpha) \end{bmatrix}, \quad (5)$$

and

$$\mathbf{R}_{x''} = \begin{bmatrix} 1 & 0 & 0 \\ 0 & \cos(\beta) & -\sin(\beta) \\ 0 & \sin(\beta) & \cos(\beta) \end{bmatrix}. \quad (6)$$

$\mathbf{R}_z$ is a rotation by θ about the z-axis to the coordinate axes (x',y',z). $\mathbf{R}_{y'}$ is a rotation by α about the y'-axis to the new coordinate axes (x'',y',z'). $\mathbf{R}_{x''}$ is a rotation by β about the x''-axis, giving the final rotated axes (x'',y'',z'').

Suppose that the noise-free unrotated data in array $\mathbf{F}$ are known a priori, regardless of the seafloor conductivity structure and regardless of the receiver's location with respect to the transmitter's tow-path. The receiver's rotation angles can then be estimated by solving the minimization problem

$$\min_{\mathbf{R}} \|\hat{\mathbf{F}}'' - \hat{\mathbf{F}}\mathbf{R}\|_F^2 \text{ subject to } \mathbf{R}^T\mathbf{R} = \mathbf{I}, \quad (7)$$

where $\mathbf{I}$ is the identity matrix and the Frobenius norm $\|\mathbf{A}\|_F^2 = \mathrm{tr}(\mathbf{A}^T\mathbf{A})$. Here, the data arrays are normalized using $\hat{\mathbf{F}}'' = \mathbf{W}\mathbf{F}''$ and $\hat{\mathbf{F}} = \mathbf{W}\mathbf{F}$, where the weighting function $\mathbf{W}$ is a diagonal matrix of the inverse data standard errors that serves to reduce the contribution of noisy data.

This minimization is referred to as the orthogonal Procrustes problem. A more generalized form that also allows for scaling and translation (and hence inspired the method's macabre name) is commonly encountered in data-alignment problems for statistics, rigid-body rotations, and image analysis (e.g., Gower, 1975; Goodall, 1991; Challis, 1995). Schönemann (1966) presents a generalized solution to the orthogonal Procrustes problem, which is simply

$$\mathbf{R}^* = \mathbf{V}[\mathrm{diag}(1,1,\det(\mathbf{V}\mathbf{U}^T))]\mathbf{U}^T, \quad (8)$$

where the columns of $\mathbf{U}$ and $\mathbf{V}$ are orthonormal vectors from the singular-value decomposition

$$\hat{\mathbf{F}}''^T\hat{\mathbf{F}} = \mathbf{U}\mathbf{S}\mathbf{V}^T, \quad (9)$$

and $\mathbf{S}$ is a diagonal matrix of singular values. The diagonal matrix in equation 8 ensures that $\det(\mathbf{R}^*) = 1$, and therefore that $\mathbf{R}^*$ performs rotation rather than reflection or rotoinversion. A derivation of the orthogonal Procrustes solution shown above and a review of the singular value decomposition are given in Golub and Van Loan (1996).

Using the notation r_{ij} for the elements of $\mathbf{R}^*$, the optimal rotation angles are then

$$\theta = \tan^{-1}\left(\frac{r_{21}}{r_{11}}\right), \quad (10)$$

$$\alpha = \sin^{-1}(r_{31}), \quad (11)$$

and

$$\beta = \tan^{-1}\left(\frac{r_{32}}{r_{33}}\right), \quad (12)$$

where it is assumed that the receiver does not land upside down so that $-\frac{\pi}{2} < \alpha, \beta < \frac{\pi}{2}$, and where using the numerical atan2 function allows for θ in all four quadrants. For the simplified case in which only the horizontal rotation is considered, $\mathbf{F}$ and $\mathbf{F}''$ will contain only the (x,y) field components. The rotation matrix is then

$$\mathbf{R} = \begin{bmatrix} \cos(\theta) & -\sin(\theta) \\ \sin(\theta) & \cos(\theta) \end{bmatrix}, \quad (13)$$

and the optimal horizontal rotation is found using equation 10. For the remainder of this study, this method will be referred to as orthogonal Procrustes rotation analysis (OPRA).

Joint inversion for receiver orientations and seafloor conductivity

For real survey data, the unrotated field vector $\mathbf{F}$ is unknown a priori, and thus the OPRA method cannot be directly used to estimate the receiver's orientation. However, the goal of a CSEM survey is to estimate seabed conductivity, and once the conductivity structure has been determined, an estimate of the unrotated fields $\mathbf{F}$ can be computed numerically. This suggests that it might be possible to simultaneously solve for the receiver orientation and the seabed conductivity using a joint inversion method. Although the inversion

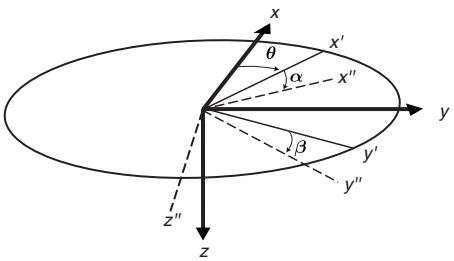

Figure 2. Rotation parameters for the absolute orientation of a CSEM receiver along orthogonal axes (x'',y'',z''). θ is the horizontal rotation about the z-axis from the survey reference axes (x,y,z) into axes (x',y',z). The receiver can be further rotated by tilt angles α and β, which describe the rotations about the y'- and x''-axes, respectively. Note that α describes tilt in a vertical plane oriented along θ, whereas angle β describes tilt along a dipping plane when $\alpha \neq 0$. The circle denotes the horizontal plane.

could be parameterized to include the receiver orientation angles, the availability of the Procrustes technique suggests a simpler possibility. **F** can be iteratively approximated with the model response of each inversion iteration, and then **R** can be estimated by using the OPRA method. The objective of such an inversion scheme is to minimize the functional

$$U = \|\partial \mathbf{m}\|^2 + \mu^{-1}[\|\mathbf{W}(\mathcal{R}^T(\mathbf{d}) - \mathcal{F}(\mathbf{m}))\|^2 - \chi_*^2], \quad (14)$$

which is a slightly modified form of the functional used in Occam's inversion (Constable et al., 1987). The first term is a spatial gradient measure of the model conductivity vector **m** and serves to stabilize the inversion, **d** is the vector of electric- and magnetic-field data, and $\mathcal{F}(\mathbf{m})$ is the model forward response in the survey coordinate axes. $\mathcal{R}^T$ is an operator that applies the transpose of the rotation matrix $\mathbf{R}^T$ to the data so that it is aligned with the survey coordinate axes; χ_*^2 is the target misfit, and μ^{-1} is a Lagrange multiplier that serves to balance the trade-off between the data fit and the model roughness.

For the studies presented here, this functional is minimized using Occam's method (Constable et al., 1987). However, the OPRA method is general and could easily be inserted into other minimization techniques commonly used for CSEM inversions. The nonlinear minimization of equation 14 is accomplished by iteratively solving for a sequence of models that produce a better fit to the data. After linearizing about an initial model $\mathbf{m}_k$, the equation for the next model in the sequence $\mathbf{m}_{k+1}$ is

$$\mathbf{m}_{k+1} = [\mu(\partial^{\mathbf{T}}\partial) + (\mathbf{W}\mathbf{J}_k)^{\mathbf{T}}\mathbf{W}\mathbf{J}_k]^{-1}[(\mathbf{W}\mathbf{J}_k)^{\mathbf{T}}\mathbf{W}\hat{\mathbf{d}}], \quad (15)$$

where

$$\hat{\mathbf{d}} = \mathcal{R}^T(\mathbf{d}) - \mathcal{F}(\mathbf{m}_k) + \mathbf{J}_k\mathbf{m}_k. \quad (16)$$

$\mathbf{J}_k$ is the linearized model response gradient or Jacobian matrix, with elements

$$J_{ij} = \frac{\partial \mathcal{F}_i(\mathbf{m}_k)}{\partial \log_{10} \sigma_j}, \quad (17)$$

where $i = 1,\ldots,n$, $j = 1,\ldots,m$; n is the number of data; and m is the number of model layers. Here, Occam's inversion method is performed in the usual way, but for each calculation in the search for the optimal μ, the operator $\mathcal{R}^T$ is found by determining each receiver's rotation matrix $\mathbf{R}^*$ using the OPRA method. This is accomplished by assigning **F** as the current model's forward response $\mathcal{F}(\mathbf{m}_k)$ and solving equation 8 for each receiver's orientation. The data are then rotated by $\mathcal{R}^T$ before the misfit is computed.

This approach is general and requires no assumptions about the receiver's location with respect to the transmitter's towpath, nor does it place assumptions on the dimensionality of the conductivity structure. The data vector **d** can contain data from a single rotated receiver or from many receivers, with some subsets having unknown orientations and the remaining receivers having known orientations. The only restriction for this method is that the data must contain both x and y horizontal field components (electric and/or magnetic) in order to determine the horizontal rotation θ. In addition, the possibly tilted vertical components (electric and/or magnetic) are needed if the tilt angles α and β are of interest. The OPRA method has been incorporated into the 1D CSEM implementation of Occam's inversion described in Key (2009), and this code is used in the following examples.

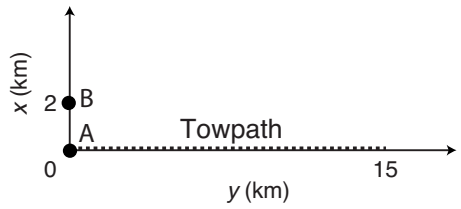

Figure 3. Location of receivers A and B and the transmitter towpath used for testing the OPRA method on a 1D reservoir model.

EXAMPLE APPLICATIONS

Example with synthetic 1D data

In this section, the OPRA method is tested on synthetic data generated for the canonical 1D reservoir model (Constable and Weiss, 2006), which is a 100-m-thick, 100-ohm-m reservoir embedded 1000 m below the seafloor in 1-ohm-m sediments and with a 1-km ocean depth. Synthetic rotated and noisy data were generated for the two receivers shown in Figure 3. Site A is located inline with the transmitter towpath and site B is located broadside at 2 km off the towpath. The synthetic data consist of vector electric and magnetic fields for 0.25-Hz horizontal electric dipole transmissions spaced at 200-m intervals. The data have been rotated using $\theta = 120°$, $\alpha = -10°$, and $\beta = 15°$. To simulate measurement uncertainties caused by noise and positioning errors, 5% vector amplitude random noise was applied independently to the real and imaginary components of the complex data. Data with amplitudes below noise floors of 10^{-15} V/Am^2 and 10^{-18} T/Am were eliminated from the data set. The inversion model consists of 75 layers spanning from the seafloor to a depth of 4.5 km. To study the performance of the OPRA method, the synthetic data for sites A and B were divided into three subsets consisting of (1) electric fields, (2) magnetic fields, and (3) electric and magnetic fields. All subsets were fit to an rms misfit of 1.0 within 30 Occam iterations. Table 1 shows the OPRA orientation results from the final Occam iteration, and Figure 4 shows the resulting inversion models.

The orientation estimates from inverting electric and magnetic fields simultaneously are within 1° of the true orientations for both sites A and B. The inversion of only electric fields worked nearly as well for both receivers, although the β angle for site B has a slightly

Table 1. Performance of OPRA as a function of site position and inverted fields. All inversions fit the data to rms 1.0 within 30 Occam iterations. The rotation angles are defined in Figure 2 and are given in degrees.

Site	Inverted fields	θ	α	β
A	Electric	120.11	−9.67	15.58
A	Magnetic	119.35	2.96	7.58
A	Electric and magnetic	120.12	−9.94	14.92
B	Electric	120.46	−10.01	16.53
B	Magnetic	120.58	−10.08	15.42
B	Electric and magnetic	120.63	−10.12	15.41
	Truth:	120.00	−10.00	15.00

larger error of 1.5°. For site A, the magnetic-field inversion performed well for estimating θ, but it exhibited 13° and 7° errors for the tilts. Conversely, the magnetic-field inversion for site B recovered all angles to within 1° error.

The relative accuracies of the orientation estimates are well explained by considering the vector geometry of the unrotated field components at each receiver. Site A is inline with the transmitter towpath and has nonzero B_x, E_y, and E_z field components, whereas all other components are at the synthetic-noise level. The field geometry at site B is more complicated. At far source-receiver offsets, site B is relatively inline with the transmitter, and the B_x, E_y, and E_z components are dominant. At short offsets, site B is essentially broadside to the transmitter and has strong B_x, E_y, and B_z components. At intermediate offsets, the field geometry is more complex, and site B has strong amplitudes for all field components. The rich geometry of field components at site B results in accurate orientation estimates for all three subsets of fields shown in Table 1.

Conversely, site A performs poorly at estimating the tilts when only magnetic fields are inverted because it exhibits linear polarization with only a single nonzero vector component (B_x). Because the other components are essentially zero (at the synthetic-noise level), the α error of 13° results in only a 2.5% difference in the amplitude of B_x. Likewise, the β angle is almost completely unconstrained because it affects only the plane of data orthogonal to B_x, which for this site is dominated by the synthetic noise. In contrast, site A worked well for inversion of only electric-field data because it contains two nonzero components that are polarized in the vertical plane along y, which allows the OPRA technique to obtain good estimates of both the horizontal rotation and the tilts.

The inversion models for each data subset (Figure 4) recover the presence of the reservoir layer, consistent with the individual field-component resolution studies presented in Key (2009).

Example with synthetic 2D data

The previous example demonstrated that inline and off-line receiver orientations can be recovered accurately for a 1D conductivity structure. However, 1D responses are often a poor approximation for finite-width 2D and 3D reservoirs (e.g., Constable and Weiss, 2006; Orange et al., 2009), and the performance of the OPRA method should be considered for such higher-dimensional structures. Although in principle the OPRA method can be inserted into 2D and 3D inversion codes, at the present time, a higher-dimensional inversion code is unavailable to the authors for such tests. Instead, this section examines how the OPRA method and 1D inversion can be used to estimate the receiver orientations when the underlying conductivity structure is 2D. Such an approximate method may prove to be useful for rapidly determining receiver orientations before undertaking the computationally intensive task of higher-dimensional inversion, which often can require several days of CPU time on large cluster computers.

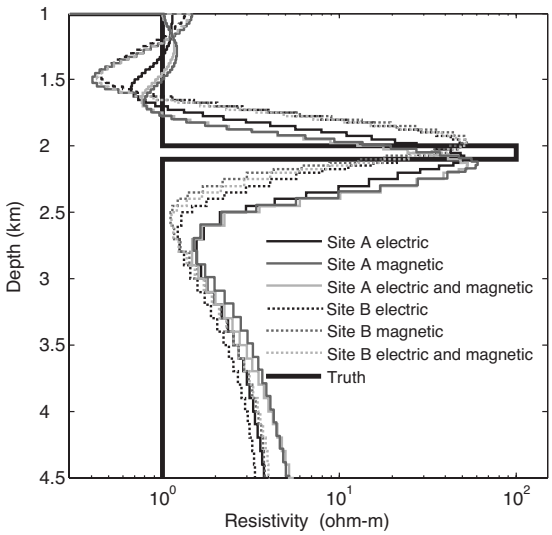

Figure 4. Occam inversion models obtained during the joint inversion for conductivity and receiver orientation for the results given in Table 1. All inversions fit 0.25-Hz transmission data to rms 1.0.

For this test, synthetic data were generated for the canonical 2D reservoir model presented in Orange et al. (2009). This model consists of a 5-km-wide, 100-m-thick, 100-ohm-m reservoir embedded in 1-ohm-m sediments at a depth of 1 km below a 1-km-deep ocean. Figure 5 shows a map-view plot of the model and the location of four receivers under consideration. Sites A and D are over the middle of the 2D reservoir, whereas sites B and C are 2 km off the left edge of the reservoir.

To make our test more representative of difficulties encountered in real surveys over unknown seafloor geology, we modeled a transmitter towpath oriented at a 48° angle to the 2D reservoir and crossing through sites B and D. Synthetic 0.25-Hz data with 5% random noise were generated for transmitters located every 500 m along the towpath to distances 15 km distal to sites B and D. Data below noise floors of 10^{-15} V/Am^2 and 10^{-18} T/Am were eliminated from the inverted data set. All four sites were rotated using the same rotations for the previous example: $\theta = 120°$, $\alpha = -10°$, and $\beta = 15°$. Both electric- and magnetic-field data were used in the inversion tests, and the data for each site were inverted separately.

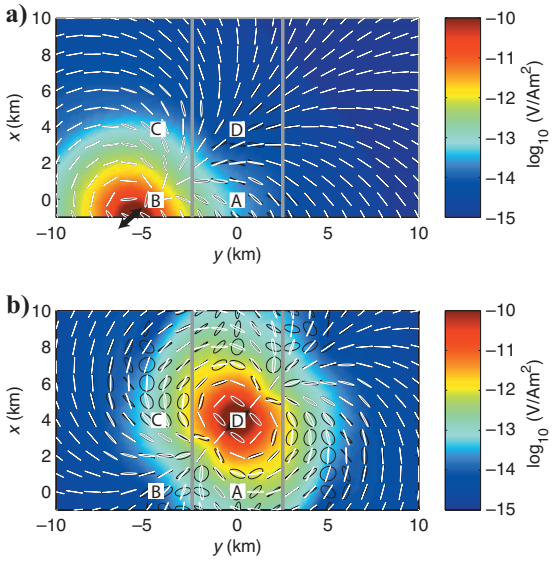

Figure 5. A map-view plot of the canonical 2D model (vertical gray lines) and the location of four seafloor EM receivers used for the tests (A through D). Shaded colors indicate the strength of the horizontal electric-field polarization-ellipse maximum for (a) a transmitter located a few kilometers to the left of the reservoir edge and (b) a transmitter over the middle of the reservoir at site D. The transmitter locations and orientations are indicated by black arrows. Electric-field polarization ellipses are shown for the 2D model (black) and for a 1-ohm-m half-space (white).

We performed a series of OPRA inversions using data with various subsets of source-receiver offsets to study which ranges would work best for 1D OPRA inversion of higher-dimensional data. To mimic real survey data, we omitted data at ranges less than 1 km, where uncertainties in transmitter position could corrupt the orientation estimates.

The orientation estimates and 1D-inversion rms misfits for each site are shown in Table 2. For each inversion, the lowest possible misfit was usually obtained within 5–10 Occam iterations, and the inversion was halted when additional iterations could not further reduce the misfit. In general, all inversions proceeded stably, and the final angles were found to within a few degrees by the end of the first or second Occam iteration. As expected, the rms misfits generally indicate that the 1D inversion does a poor job of fitting the 2D data. Somewhat surprisingly, most of the orientation estimates are within a few degrees of the true orientations, even for the sites with a large misfit.

For the subset of data at ranges greater than 1 km, the error in the angles is less than 4°, except for the 8° error in α at site A. We tried using data only in a range of 1 to 4 km under the premise that such shorter offsets might be limited in sensitivity to the 2D reservoir. Although off-target sites B and C were still recovered to within 4°, on-target sites A and D now have larger orientation errors (as much as 13°) than when all the data were included, suggesting that some 2D effects are corrupting these estimates.

Because higher-dimensional effects would be difficult to identify and omit for real survey data without a priori knowledge of the seabed conductivity and reservoir geometry, we seek another subset of data for improving the orientation estimates. Visual inspection of the synthetic data showed flat phases indicative of the so-called airwave beginning at about a 7-km range. Because such long-offset data increasingly becomes dominated by energy that propagates along the air-sea interface, it seems likely that these data would be relatively less sensitive to the corrupting effects of deeper 2D structure than the shorter-offset data. As shown by the last four entries in Table 2, this is indeed the case. When only long-offset data are used, sites A and D are significantly improved over the shorter-offset OPRA inversion, and now all angles at all sites are accurate to within 3° and many of them to within 1°.

Some insight on this unexpected good performance can be gained by considering the geometry of the transmitted fields. Figure 5 shows a map-view plot of the seafloor horizontal electric-field polarization ellipses for the canonical 2D model and for a uniform 1-ohm-m half-space seafloor. When the transmitter is off the target (Figure 5a), the polarization ellipses for the 2D model are aligned with the half-space ellipses throughout the survey region, except for several degrees of difference over the reservoir near sites A and D. When the transmitter is positioned over the reservoir (Figure 5b), the 2D ellipses are dramatically different than the half-space ellipses both over the reservoir and as much as several kilometers off the reservoir. Therefore, 2D effects are present in the data at 4-km range for sites A and D, and that is why the shorter-range data performed less well for these two sites. At ranges greater than about 7 km, the ellipses have good alignment with the half-space ellipses because the energy becomes dominated by the airwave, hence illustrating why long-range data OPRA inversions performed well.

Table 2. Performance of the OPRA method for 1D inversion of 2D data from the four sites shown in Figure 5. The range column denotes various subsets of source-receiver offsets used in the OPRA inversions.

Site	Range (km)	rms misfit	θ	α	β
A	$1 \le r$	5.65	123.13	−2.26	16.89
B	$1 \le r$	2.95	123.35	−10.07	15.93
C	$1 \le r$	5.36	119.08	−9.84	11.90
D	$1 \le r$	5.16	123.09	−9.62	14.69
A	$1 \le r \le 4$	4.72	130.26	3.13	23.20
B	$1 \le r \le 4$	1.26	123.80	−8.68	16.37
C	$1 \le r \le 4$	1.26	121.76	−10.48	13.19
D	$1 \le r \le 4$	5.02	115.53	−9.42	15.23
A	$7 \le r$	2.65	119.94	−13.16	15.28
B	$7 \le r$	3.06	123.16	−11.01	13.67
C	$7 \le r$	6.35	119.45	−7.45	17.26
D	$7 \le r$	2.41	119.78	−10.30	14.99
		Truth:	120.00	−10.00	15.00

Comparison with previously oriented survey data

Here we apply the OPRA method to the field data previously considered for orientation estimation in Mittet et al. (2007). In that work, the receiver orientation was determined by a search method that finds the horizontal rotation that minimizes the crossline electric-field component. The polarization-ellipse study shown in Figure 1a demonstrates that this is a reasonable assumption for an inline transmitter tow. The data set consists of horizontal electric and magnetic fields for a single receiver and an inline transmitter tow at a geographic azimuth of 74.3° from north. Mittet et al. (2007) find the receiver rotation to be 44° from the towline but then apply a 180° correction to match the observed phases. The corresponding geographic orientation θ is −61.7°. The results of the OPRA method as a function of Occam iterations are shown in Table 3. After six iterations, the target misfit of 1.9 was obtained and the resulting orientation angle is −61.3°, in good agreement (a 0.4° difference) with the angle found by Mittet et al. (2007). The results for each iteration show that this angle was found to within 0.2° on the first iteration, even though the model-response misfit was still relatively large (rms 7.6).

Application to CSEM data from offshore northwest Australia

Our final example demonstrates how the OPRA method can be applied to real survey data. We examine CSEM data collected over the Pluto gas field on the North West Shelf of Australia, 190 km northwest of Karratha. Pluto and the nearby Xena field together comprise a 5 TCF gas accumulation (Tilbury et al., 2009). The discovery well (Pluto-1) targeted a seismic-amplitude anomaly extending from a region of poor seismic imaging associated with the steep continental-slope bathymetry. The main reservoir sand is approximately 3100 m below sea level in a tilted Triassic fault block. The discovery well intersect-

ed a gross gas column 209 m thick, and petrophysical analysis confirmed an average net porosity of 28% and average gas saturation in the main reservoir of 93%.

Table 3. Performance of OPRA as a function of Occam iterations for the sample EMGS data. The inversion reached the target misfit of 1.9 in six iterations.

Iteration	rms misfit	θ
1	7.627	−61.47
2	7.029	−61.45
3	5.376	−61.33
4	2.760	−61.29
5	2.019	−61.27
6	1.900	−61.27

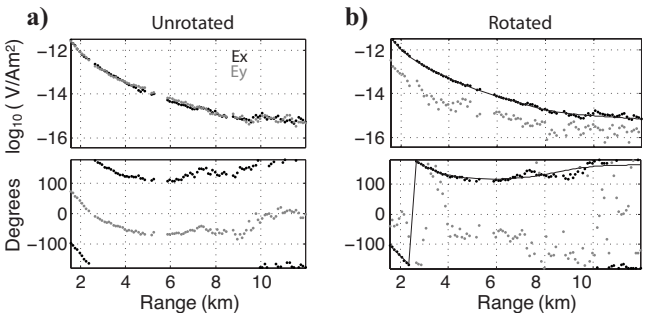

Figure 6. Amplitude and phase for 0.24-Hz electric-field data (a) before and (b) after rotation to the survey line. The solid line shows the inline electric-field response for the smooth inversion model shown in Figure 7.

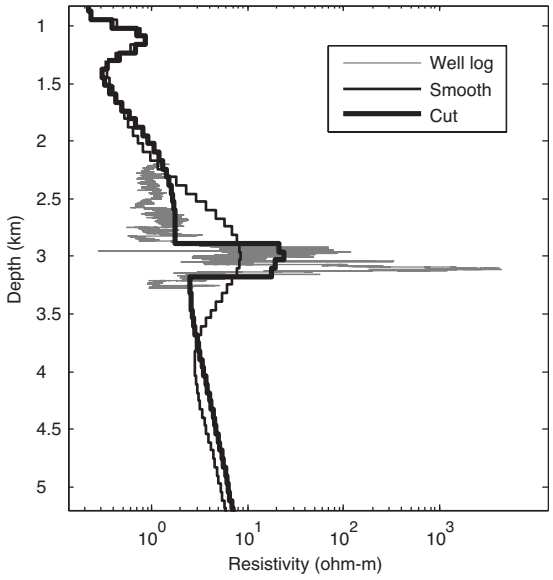

Figure 7. Inversion models obtained from inverting 0.24- and 0.4-Hz inline electric-field and crossline magnetic-field data. Both smooth (thin line) and penalty-cut inversions (thick line) fit the data to rms 1.0 and agree well with location of the reservoir in the Pluto-1 well log (gray line).

The combination of thick, high-porosity reservoir sands and high hydrocarbon saturation encountered in Pluto-1 made the Pluto field a suitable candidate for the CSEM method. Although the seismic-imaging difficulties caused by the continental slope and deeply incised canyons were subsequently resolved by the application of prestack depth migration, a single line of CSEM data represents a comparable exploration investment. Therefore, in early 2007, CSEM data were acquired over the Pluto gas field to test the viability of CSEM as an exploration tool in conditions where seismic imaging is challenging.

The survey data considered here consists of 0.24-Hz and 0.4-Hz horizontal electric- and magnetic-field data recorded by a single inline receiver located over the reservoir. Figure 6 shows the unrotated 0.24-Hz electric-field data, which have considerably larger scatter than that observed for other surveys using the same contractor. Before running the inversion, data points with strong deviations from the general response trend were removed, and an error floor of 5% was applied to the edited data set. We then ran the OPRA inversion on the edited data set and found a horizontal orientation angle θ of 44°. Figure 6b shows the 0.24-Hz electric-field data after rotation to inline and crossline components. As expected for an inline transmitter tow and laterally uniform overburden, the crossline data have a much lower amplitude than the inline data (the ideal would be zero amplitude for perfect inline geometry, 1D conductivity, and noise-free measurements).

After solving for the receiver orientation, we rotated the vector data to the survey-line direction and inverted only the inline electric field and the crossline magnetic field. Figure 7 shows the resulting inversion model computed using the first-derivative roughness penalty for the regularization. This smooth inversion can detect a resistivity increase in the vicinity of the reservoir, but the anomaly is highly smeared out in depth because of nonuniqueness inherent in a finite noisy data set and because CSEM data is primarily sensitive to the resistivity-thickness product for deeply buried thin resistors (e.g., Constable and Weiss, 2006). By incorporating the known gas horizon depths into the inversion, some of this nonuniqueness can be mitigated. Figure 7 also shows a penalty-cut inversion, in which the model roughness penalty has been removed along the top and bottom of the gas horizon. The cut inversion model has much better agreement with the well log in terms of the background resistivity trend and overall reservoir resistivity.

CONCLUSIONS

We have presented the orthogonal Procrustes rotation analysis (OPRA) method and shown how it can be used to reliably estimate the orientation of seafloor EM receivers. The OPRA method works by solving a minimization problem for the optimal rotation matrix that relates the recorded field data to predicted field data. This minimization is embedded in a nonlinear inversion routine that iteratively searches for both the optimal receiver rotation and a conductivity model that are compatible with the observed data.

Our synthetic tests of the OPRA method embedded into the Occam1DCSEM inversion demonstrate that it can produce orientation estimates accurate to about 1° for inline and broadside synthetic data from a simple 1D reservoir model. Inline site orientations were best determined when using electric-field data or both electric- and magnetic-field data. When only magnetic fields were inverted, the horizontal rotation was accurately recovered, but the tilts contained as much as several degrees of error because they are not well con-

strained by the linear crossline polarization of the magnetic field. Because broadside receivers contain a rich mixture of field geometries, inverting either magnetic- or electric-field data produced reliable orientation angles.

For synthetic 2D data, we found that receiver orientation estimates were less accurate when the transmitter is over the reservoir, producing a strong 2D distortion incompatible with the 1D inversion. We found that a simple solution is to use only large-offset data, which tend to be dominated by the airwave and hence is less sensitive to 2D distortion. Our example application to the Pluto gas field CSEM data illustrated how real survey data can be oriented with the OPRA method and then subsequently inverted to produce a useful resistivity profile of the gas reservoir.

There are probably field data sets in which the OPRA method will need to be applied carefully so as to produce reliable orientations. For example, in strongly heterogeneous regions, the method may need to be embedded into 2D or 3D inversion codes or those that can handle the field distortions produced by anisotropic conductivity. However, our experience with the data examples studied here and with other field data sets not shown here suggests that the OPRA method can often yield reliable orientations when applied with 1D inversion.

ACKNOWLEDGMENTS

We thank Rune Mittet and EMGS for providing the field data used in Table 3 and Woodside Energy for providing permission to publish the well-log and CSEM data shown in our final example. K. Key acknowledges support from the Seafloor Electromagnetic Methods Consortium at Scripps Institution of Oceanography and Woodside Energy. Rune Mittet, two anonymous reviewers, and the associate editor provided helpful review comments. The source code for the Occam1DCSEM inversion that includes the OPRA method can be freely obtained at http://marineemlab.ucsd.edu/Projects/Occam/1DCSEM.

REFERENCES

Challis, J. H., 1995, A procedure for determining rigid body transformation parameters: Journal of Biomechanics, **28**, 733–737.

Constable, S. C., A. S. Orange, G. M. Hoversten, and H. F. Morrison, 1998, Marine magnetotellurics for petroleum exploration, Part I: A sea-floor equipment system: Geophysics, **63**, 816–825.

Constable, S. C., R. L. Parker, and C. G. Constable, 1987, Occam's inversion: A practical algorithm for generating smooth models from electromagnetic sounding data: Geophysics, **52**, 289–300.

Constable, S., and L. J. Srnka, 2007, An introduction to marine controlled-source electromagnetic methods for hydrocarbon exploration: Geophysics, **72**, no. 2, WA3–WA12.

Constable, S., and C. J. Weiss, 2006, Mapping thin resistors and hydrocarbons with marine EM methods: Insights from 1D modeling: Geophysics, **71**, no. 2, G43–G51.

Edwards, N., 2005, Marine controlled source electromagnetics: Principles, methodologies, future commercial applications: Surveys in Geophysics, **26**, 675–700.

Ellingsrud, S., T. Eidesmo, S. Johansen, M. C. Sinha, L. M. MacGregor, and S. Constable, 2002, Remote sensing of hydrocarbon layers by seabed logging (SBL): Results from a cruise offshore Angola: The Leading Edge, **21**, 972–982.

Golub, G. H., and C. F. Van Loan, 1996, Matrix computations, 3rd ed.: Johns Hopkins University Press.

Goodall, C., 1991, Procrustes methods in the statistical analysis of shape: Journal of the Royal Statistical Society Series B, **53**, 285–339.

Gower, J., 1975, Generalized Procrustes analysis: Psychometrika, **40**, 33–51.

Key, K., 2009, 1D inversion of multicomponent, multifrequency marine CSEM data: Methodology and synthetic studies for resolving thin resistive layers: Geophysics, **74**, no. 2, F9–F20.

MacGregor, L. M., M. Sinha, and S. Constable, 2001, Electrical resistivity structure of the Valu Fa Ridge, Lau Basin, from marine controlled-source electromagnetic sounding: Geophysical Journal International, **146**, 217–236.

Mittet, R., O. M. Aakervik, H. R. Jensen, S. Ellingsrud, and A. Stovas, 2007, On the orientation and absolute phase of marine CSEM receivers: Geophysics, **72**, no.4, F145–F155.

Orange, A., K. Key, and S. Constable, 2009, The feasibility of reservoir monitoring using time-lapse marine CSEM: Geophysics, **74**, no. 2, F21-F29.

Schönemann, P., 1966, A generalized solution of the orthogonal Procrustes problem: Psychometrika, **31**, 1–10.

Smith, B. D., and S. H. Ward, 1974, On the computation of polarization ellipse parameters: Geophysics, **39**, 867–869.

Tilbury, L. A., C. J. Clayton, T. J. Conroy, G. Philip, G. A. Boyd, G. G. Johnson, M. A. Rayfield, L. Hartanto, and D. P. Lance, 2009, Pluto — A major gas field hidden beneath the Continental Slope (DVD): The APPEA Journal, **49**, 243–265.

Weitemeyer, K. A., S. C. Constable, K. W. Key, and J. P. Behrens, 2006, First results from a marine controlled-source electromagnetic survey to detect gas hydrates offshore Oregon: Geophysical Research Letters, **33**, L03304, doi: 10.1029/2005GL024896.